Comprehensive model for ideal reverse leakage current components in Schottky barrier diodes tested in GaN-on-SiC samples

B. Orfao,[1,a)] G. Di Gioia[2], B. G. Vasallo,[1] S. Pérez,[1] J. Mateos,[1] Y. Roelens[2], E. Frayssinet[3], Y. Cordier[3], M. Zaknoune,[2] and T. González[1]

[1] *Dpto. Física Aplicada and USAL-NANOLAB, Universidad de Salamanca, 37008 Salamanca, Spain*

[2] *CNRS-IEMN, Université de Lille, UMR8520, Av. Poincaré, 59650 Villeneuve d'Ascq, France*

[3] *Université Côte d'Azur, CNRS, CRHEA, rue B. Grégory, 06560 Valbonne, France*

Abstract: A model to predict the ideal reverse leakage currents in Schottky barrier diodes, namely thermionic emission and tunneling components, has been developed and tested by means of current-voltage-temperature measurements in GaN-on-SiC devices. The model addresses both forward and reverse polarities in a unified way and with the same set of parameters. The values of the main parameters (barrier height, series resistance and ideality factor) are extracted from the fitting of the forward-bias *I-V* curves, and then used to predict the reverse-bias behavior without any further adjustment. An excellent agreement with the *I-V* curves measured in forward bias in the GaN diode under analysis has been achieved in a wide range of temperatures (275-475 K). In reverse bias, at temperatures higher than 425 K a quasi-ideal behavior is found, but additional mechanisms (most likely trap-assisted tunneling) lead to an excess of leakage current at lower temperatures. We demonstrate the importance of the inclusion of image-charge effects in the model in order to correctly predict the values of the reverse leakage current. Relevant physical information, like the energy range at which most of the tunnel injection takes place, or the distance from the interface at which tunneled electrons emerge, is also provided by the model.

[a)] Author to whom correspondence should be addressed. Electronic mail: beatrizorfao@usal.es

I. INTRODUCTION

Schottky barrier diodes (SBDs) have demonstrated excellent high-frequency performance, which has allowed the fabrication of RF sources reaching the THz range[1] or building sensitive direct detectors of THz radiation at room temperature.[2,3] In the last years, wide-bandgap semiconductors like SiC and GaN have started to be used for the fabrication of SBDs oriented to high-power applications, which have today a broad field of purposes like the production of on-board battery chargers and off-board charging stations for the electric vehicle industry,[4,5] DC/DC boost converters and DC/AC inverters for solar and renewable energy applications,[6] etc.

GaN-based devices have already demonstrated good performances for high-power, high-frequency and high-temperature electronics, mainly using the classical HEMT technology.[7] GaN SBDs are also believed to be suitable for the next generation of high-power circuits.[8] They could offer high switching speed and low reverse recovery loss in switched-mode power supplies, thus competing with SiC SBD technology, as well as challenge the power handling capabilities of the standard GaAs technology used in sub-THz multipliers.[9] However, issues related to defects that originate a high reverse leakage current, degrading their breakdown voltage and reliability, have hindered the use of GaN SBDs for practical applications.[10] The modelling of carrier transport through the metal-semiconductor rectifying contact is essential to identify the origin of the technological problems and find solutions for the exploitation of GaN SBDs in modern electronic applications. Additionally, the in-depth knowledge of these contacts is essential in understanding other semiconductor devices, like field effect transistors, where they act as gate terminal, controlling the electrical performance of devices.

The dominant current mechanism in the forward-bias current of SBDs is thermionic emission over the energy barrier formed at the metal-semiconductor interface.[11] But the electrical properties of fabricated devices deviate from the fundamental theory, and additional fitting parameters like the ideality factor and the series resistance are necessary to correctly reproduce the experimental I-V curves.[12,13,14] In reverse bias, ideally, in addition to thermionic emission, tunneling current becomes important.[13] This leakage current contribution affects the high-power operation of SBDs and degrades their breakdown characteristics.[15] The widely accepted models by Murphy and Good[16] and Padovani and Stratton[17] provide analytical expressions for the current only applicable in some specific ranges of reverse bias. Here, one of the difficulties is the inclusion of image charge (IC) effects, with the associated barrier lowering, necessary to determine precisely the reverse current at low

values of the surface electric field, when the shape of the barrier top is of importance. Analytical expressions by means of a trapezoidal approximation for the barrier have been derived in the literature.[18,19]

However, deviations from these two (thermionic-emission and tunneling) ideal current components are regularly observed in reverse bias. In some cases, mainly in non-mature technologies, current values much higher than expected are measured, leading to a premature breakdown of the devices.[20] The (non-ideal) additional contributions to the reverse leakage current can be due to interface or deep-level defects and dislocations. These effects can be especially important in GaN SBDs and related wide bandgap devices because of their relatively high defect density.[10] Mechanisms such as trap-assisted tunneling, Poole-Frenkel emission or variable-range hopping have been typically identified as sources of leakage current in GaN SBDs.[20,21,22,23,24] Enhanced performance has been achieved by appropriate growing conditions,[25] surface treatments[26] or contact terminations.[21,27]

In order to assess how ideal is the behavior of SBDs in reverse bias and evaluate correctly the excess current contributions associated to other leakage mechanisms, the development of an accurate model for thermionic emission and tunneling currents is essential. Such a model should be consistent with the behavior of the diode in forward bias, this is, described by the same parameters in both polarities, which requires to address them simultaneously.[18] In this work, we develop a comprehensive unified model for thermionic and tunneling currents describing transport in both polarities with a single set of physically meaningful parameters, determined from the fitting of the *I-V* curve in forward bias and then applied to predict the diode behavior in reverse bias (with no other adjustable factors). The model includes a detailed numerical treatment of IC, shown to be necessary to reproduce experimental results, and the influence of the epilayer doping in the shape of the barrier. Current-voltage-temperature characteristics measured in GaN-on-SiC SBDs fabricated at IEMN[28] have been used to validate the model, finding always an excellent agreement in forward bias and also for the highest temperatures in reverse bias, thus corroborating the good quality of the technological process used. For temperatures below 400 K, leakage current in excess is observed and attributed to trap assisted tunneling.

The paper is organized as follows. The model is described in Sec. II. Experimental details about the devices and measurements are reported in Sec. III. The results and their discussion are provided in Sec. IV. Finally, the main conclusions are drawn in Sec. V.

II. MODEL

The total current in an ideal SBD is formed of two components: thermionic emission, J_{th}, and tunneling, J_{tunnel}. In forward bias, as long as the Schottky layer is moderately doped, the current is essentially due to thermionic emission, and J_{tunnel} can be neglected; while in reverse bias, depending on the applied voltage V, both contributions may be of importance. Thus, in our model we will consider the current components shown in Fig. 1, corresponding to the thermionic emission of electrons from the semiconductor to the metal $J_{th}^{s\to m}$, from the metal to the semiconductor $J_{th}^{m\to s}$, and to the tunneling of electrons from the metal to the semiconductor $J_{tunnel}^{m\to s}$.

The values of these current components for a given V depend on the height and shape of the energy barrier. Taking the metal Fermi level ε_{Fm} as the zero-energy reference, and including the influence of the IC and the doping of the active layer N_D, the potential energy in the Schottky layer at a distance x from the metal interface is given by[29,30]

$$\varepsilon_C(x) = e\phi_B - e\left[\frac{2eN_D}{\epsilon_s}(V_B - V)\right]^{\frac{1}{2}} x + \frac{e^2 N_D x^2}{2\epsilon_s} - \frac{e^2}{16\pi\epsilon_s x} , \quad (1)$$

where ϕ_B is the barrier height, V_B the built-in potential and ϵ_s the permittivity of the semiconductor. Note that the second term in Eq. (1) corresponds to $-eEx$, with E the surface electric field at the metal-semiconductor interface, the third term accounts for the influence of the doping and the last one for the lowering of the barrier due to the IC.

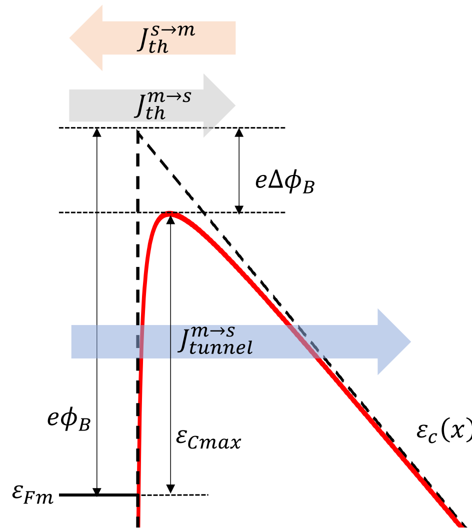

FIG. 1. Scheme of the energy barrier with and without IC corrections, and current contributions considered in the model. The arrows indicate the movement of electrons, currents flow in the opposite sense.

We will use a general formalism for the calculation of these current components. The injected current from one side of the junction into the other one in the range $d\varepsilon$ around an energy ε normal to the barrier can be written as

$$J(\varepsilon)d\varepsilon = -e \cdot N(\varepsilon) \cdot T_C(\varepsilon)d\varepsilon \,, \tag{2}$$

where

$$N(\varepsilon) = \frac{A^*T}{ek_B} \cdot \ln\left[1 + \exp\left(-\frac{\varepsilon - \varepsilon_F}{k_BT}\right)\right] \tag{3}$$

is the number of electrons per unit area incident on the barrier with normal energy ε per unit time and per unit energy[31] at the side (metal or semiconductor) from which they are injected and $T_C(\varepsilon)$ is the transmission coefficient corresponding to that energy. ε_F is the Fermi energy at the side (metal or semiconductor) from which electrons are injected, T the absolute temperature and $A^* = 4\pi m^* k_B^2 e/h^3$ the effective Richardson constant, with k_B the Boltzmann constant, m^* the electron effective mass of the semiconductor and h the Planck constant. We will consider a single effective mass for both the Richardson constant and the tunneling effective mass.[18,29] Eq. (2) assumes a negligible occupation of the states with energy ε at the side into which electrons are injected, as expected for the case of thermionic contributions (as long as the barrier is high enough) and tunneling from the metal to the semiconductor in reverse bias.

$T_C(\varepsilon) = 1$ for energies above the maximum of the barrier $\varepsilon > \varepsilon_{Cmax}$, corresponding to thermionic-emission processes, while for $\varepsilon < \varepsilon_{Cmax}$, corresponding to tunneling processes, $T_C(\varepsilon)$ is calculated using the Wentzel-Kramers-Brillouin (WKB) approximation for the evaluation of the tunneling probability as[32]

$$T_C(\varepsilon) = \exp\left[-\frac{2}{\eta}\int_{x_1}^{x_2}\sqrt{2m^*(\varepsilon_c(x) - \varepsilon)}dx\right], \tag{4}$$

with x_1 and x_2 the classical turning points at which $\varepsilon_c(x) = \varepsilon$.

As shown in Fig. 1, $\varepsilon_{Cmax} = e(\phi_B - \Delta\phi)$, where $\Delta\phi = \sqrt{eE/4\pi\epsilon_s}$ is the IC lowering of the barrier (calculated neglecting the influence of N_D, third term in Eq. (1)). If IC effects are neglected, $\varepsilon_{Cmax} = e\phi_B$.

Thus, the current associated to electrons injected from the metal into the semiconductor is calculated as[29]

$$\begin{aligned} J^{m\to s} &= -e\int_{\varepsilon_{min}}^{\infty} N_m(\varepsilon)T_C(\varepsilon)d\varepsilon = -e\int_{\varepsilon_{min}}^{\varepsilon_{Cmax}} N_m(\varepsilon)T_C(\varepsilon)d\varepsilon - e\int_{\varepsilon_{Cmax}}^{\infty} N_m(\varepsilon)d\varepsilon \\ &= J_{tunnel}^{m\to s} + J_{th}^{m\to s} \end{aligned} \tag{5}$$

where ε_{min} is the minimum energy in the metal for which tunneling into the semiconductor is possible (there must be available states in the conduction band of the semiconductor at the same energy). For the sake of accuracy the calculation of $J_{tunnel}^{m\to s}$ is performed numerically, since there is no simple analytical expression for $T_C(\varepsilon)$ when IC corrections are included in the energy barrier, despite trapezoidal approximations have been reported.[18,19] In the case of $J_{th}^{m\to s}$, since the involved energies typically fulfil $\varepsilon - \varepsilon_{Fm} \gg k_B T$, it is possible to approximate

$$N_m(\varepsilon) \approx \frac{A^* T}{e k_B} \cdot \exp\left(-\frac{\varepsilon - \varepsilon_{Fm}}{k_B T}\right), \tag{6}$$

allowing to evaluate $J_{th}^{m\to s}$ analytically as

$$J_{th}^{m\to s} = -A^* T^2 \exp\left(-\frac{\varepsilon_{Cmax}}{k_B T}\right). \tag{7}$$

As explained before, the current associated to electrons injected from the semiconductor into the metal is considered to be only due to thermionic emission. Assuming no collision of electrons in the depletion region (coherent with the relatively high mobility of GaN in our case), this current is given by

$$J^{s\to m} = J_{th}^{s\to m} = e \int_{\varepsilon_{Cmax}}^{\infty} N_s(\varepsilon) d\varepsilon. \tag{8}$$

Again, since the involved energies typically fulfil $\varepsilon - \varepsilon_{Fs} \gg k_B T$, it is possible to approximate

$$N_s(\varepsilon) \approx \frac{A^* T}{e k_B} \cdot \exp\left(-\frac{\varepsilon - \varepsilon_{Fs}}{k_B T}\right). \tag{9}$$

Taking into account that $\varepsilon_{Fs} = \varepsilon_{Fm} + eV$, one arrives to

$$J_{th}^{s\to m} = A^* T^2 \exp\left(-\frac{\varepsilon_{Cmax}}{k_B T}\right) \exp\left(\frac{eV}{k_B T}\right). \tag{10}$$

The total thermionic emission current will thus be given by

$$J_{th} = J_{th}^{s\to m} + J_{th}^{m\to s} = A^* T^2 \exp\left(-\frac{\varepsilon_{Cmax}}{k_B T}\right)\left[\exp\left(\frac{eV}{k_B T}\right) - 1\right] = J_0 \left[\exp\left(\frac{eV}{k_B T}\right) - 1\right]. \tag{11}$$

In a general case with IC effects included, the reverse saturation current J_0 is $A^* T^2 \exp\left[-e\left(\phi_B - \Delta\phi_B\right)/k_B T\right]$ and thus depends on the applied voltage V through $\Delta\phi_B$.

This ideal expression for J_{th} must be further modified to include real effects, like the influence of the series resistance R_s and the ideality factor η, as

$$J_{th}(V) = J_0 \left[e^{\frac{e(V - J_{th} S R_S)}{\eta k_B T}} - 1\right], \tag{12}$$

where S is the surface of the Schottky contact. The inclusion of these two parameters, external to the ideal model, is necessary to achieve a good fitting of the forward I-V curves, essential to accurately determine ϕ_B.

The final aim of this model is to predict the ideal reverse I-V characteristics of SBDs as a function of temperature T. Six parameters are involved in the model, namely, ϕ_B, N_D, ϵ_s, m^*, R_s and η. We proceed as follows to determine their values. ϵ_s and m^* are taken from the literature ($8.9\epsilon_0$ and $0.22m_0$ for the case of GaN). We use the low-frequency permittivity for both the surface electric field and the IC term. The value of N_D is extracted from C-V measurements in reverse bias (1.05×10^{17} cm^{-3} in our case). And finally, ϕ_B, R_s and η are determined from the fitting to Eq. (12) of the experimental I-V curves measured in forward bias.

Once the values of the parameters are determined, they are used to predict the reverse I-V characteristics, including thermionic and tunneling currents, as

$$J_{reverse}(V) = J_{th}(V) + J_{tunnel}^{m\to s}(V), \qquad (13)$$

without any further fitting or adjustment of parameters.

In order to confirm the need to include the IC correction in the calculations, a fitting of the I-V curve measured in forward bias will also be performed without considering the influence of IC, thus obtaining an effective barrier height ϕ_B^{eff}, lower than the value of ϕ_B extracted when IC is considered, and the corresponding η^{eff}. Remarkably, an excellent agreement of the forward I-V curves can be attained in both ways, which could erroneously lead to believe that the reverse I-V curve should also be well predicted by both approaches. To check this fact, calculations of the reverse I-V characteristics with the full model (including IC and taking $\varepsilon_{Cmax} = e(\phi_B - \Delta\phi)$) will be compared with those ignoring IC (removing the last term in Eq. (1)) and using effective parameters ($\varepsilon_{Cmax} = e\phi_B^{eff}$) to eventually determine which is the model best fitting the experimental reverse I-V curves.

III. EXPERIMENTAL

GaN-on-SiC SBDs fabricated at IEMN have been characterized to validate the model.[28] The epitaxial layer was grown at CRHEA by metal organic vapor phase epitaxy on a semi-insulating 6H-SiC substrate. A SEM image of one of the diodes is shown in Fig. 2(a), while the details of the epitaxial layer are provided in the scheme of Fig. 2(b). A 490 nm unintentionally doped GaN was grown first, followed by a highly doped 950 nm thick GaN layer (300 nm @ 1×10^{19} cm^{-3} and 650 nm @ 2×10^{19} cm^{-3}) to achieve a good ohmic contact and a

low series resistance, and finally a 1 μm n$^-$ GaN layer (nominally 6.6×10^{16} cm^{-3}) acting as the Schottky layer. The mesa definition was made by Cl_2/Ar ICP dry etch using a 250 nm thick PECVD deposited SiO_2 mask. A standard Ti/Al/Ni/Au ohmic contact was then deposited on the n^{++} layer after surface cleaning. Next, a rapid thermal annealing was performed at 850º C for 30 s in a N_2 ambient. For the Schottky contact fabrication, the sample was treated with a BOE solution to remove the remaining SiO_2 layer and uncover the GaN surface, and a surface treatment was also performed before depositing the Pt/Au metals through e-beam evaporation on the top n$^-$ layer. The results shown in this work correspond to a circular diode with a diameter of 221 μm. The large area of the Schottky contact allows expecting a negligible influence of edge effects. Diodes with other similar sizes exhibit the same qualitative behavior.

I-*V* and *C*-*V* measurements have been performed at different temperatures by means of a LakeShore CRX-VF cryogenic probe station. The *C*-*V* measurements in reverse bias have been used to extract the doping of the epilayer, obtaining a value of 1.05×10^{17} cm^{-3} (higher than the nominal one), which will be used in our calculations. Barrier height values are also extracted from *C*-*V* measurements but, for consistency, we will adopt the values fitting the forward *I*-*V* characteristics, which, when IC effects are included, are slightly higher than those obtained from *C*-*V* curves.

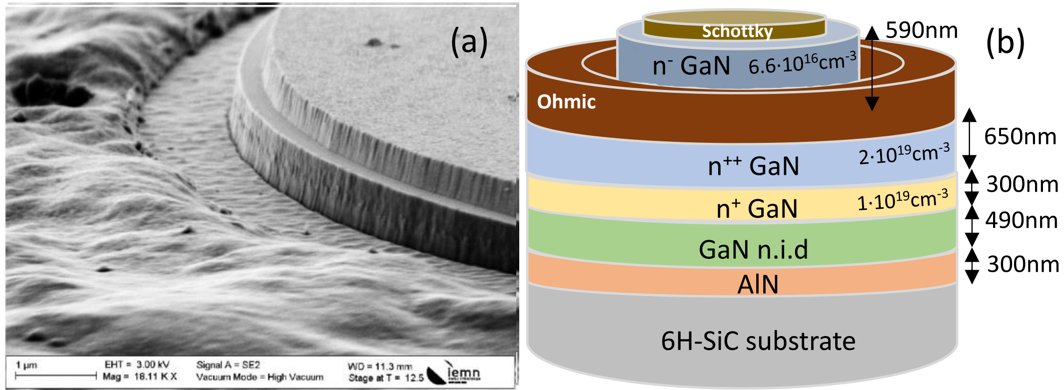

FIG. 2. (a) SEM image of a real SBD fabricated at the IEMN and (b) scheme of the epitaxial layer.

IV. RESULTS AND DISCUSSION

Current-voltage-temperature measurements were carried out from 275 to 475 K, as shown in Fig. 3 for (a) forward and (b) reverse bias. Note that the lower limit of the measurements is about 10^{-11} A. The expected increase of current with temperature is observed. As explained, the ideal model for the forward *I*-*V*

characteristics includes the thermionic emission contribution J_{th} incorporating the lowering of the barrier originated by IC. Additionally, real effects like the influence of the series resistance R_s and the ideality factor η are accounted for to provide the final expression given by Eq. (12). As observed in Fig. 3(a), our model reproduces very closely the experimental curves. From the fitting, the values of ϕ_B, η, and R_s at each temperature are determined. The inclusion of R_s, taking values around 10 Ω for all the temperatures (since the temperature-independent contact resistance is much larger than the contribution associated with the semiconductor), is essential to fit the experimental values for current levels above 10^{-4} A. The values of ϕ_B and η extracted from the fittings are provided in the inset as a function of temperature. Values of ϕ_B in the range 0.92-0.94 eV, slightly increasing with T, are obtained, while the ideality factor is always lower than 1.05 (nearly 1 for the highest temperatures), indicating the good quality of the diodes.

Once the parameters of the model have been fixed from the fitting of the forward *I-V* curves, we can use it to predict the ideal behavior of the diodes in reverse bias, where, in addition to the thermionic current, the tunnel contribution, calculated as indicated in Eq. (5), is also included. As observed in Fig. 3(b), for the highest temperatures, the results of the model practically coincide with the experimental values, thus confirming the validity of our approach and the nearly ideal behavior of the diodes. However, for temperatures below 425 K, the current values deviate from the addition of the two ideal contributions, exhibiting significantly higher values, which means that additional non-ideal leakage current mechanisms are present.

An excellent fitting (not shown) of the forward *I-V* curves, similar to that reported in Fig. 3(a), can also be obtained if IC effects are ignored in the model and different values of the barrier height and ideality factor are used, ϕ_B^{eff} and η^{eff} respectively, denoted as effective parameters (also shown in the inset of Fig. 3(a) as NoIC-EP case). As expected, ϕ_B^{eff} is systematically lower than ϕ_B to afford the same current level in the absence of IC barrier lowering. On the other hand, η^{eff} lies in the range 1.05-1.10, thus exhibiting a slightly higher deviation from ideality than when IC is considered.

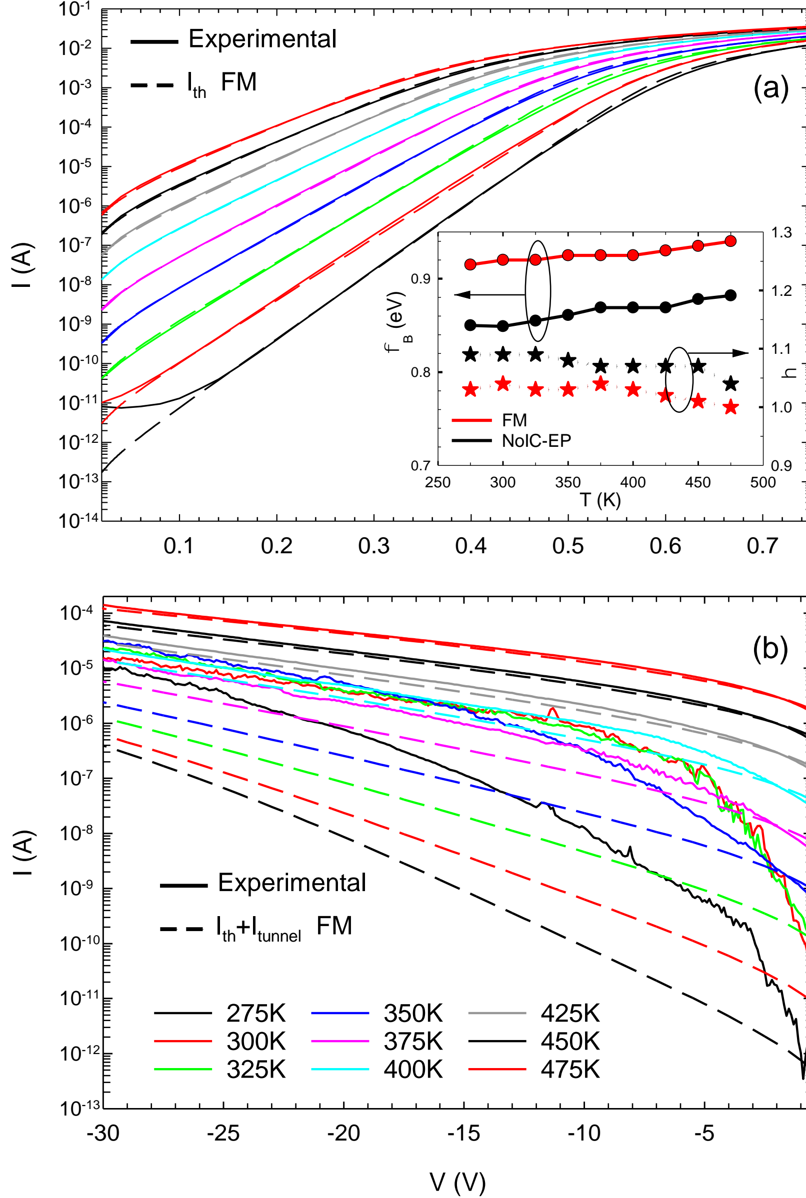

FIG. 3. Measured (solid lines) and modelled (dashed lines) *I-V* curves for (a) forward and (b) reverse bias. The (full) model includes thermionic emission and tunneling currents (the latter only in reverse bias) with the influence of IC and R_s. Inset: ϕ_B and η extracted by fitting the full model (FM) to the experimental curves in forward bias; the values of the effective parameters ϕ_B^{eff} and η^{eff} fitting the forward *I-V* curves in the absence of IC effects (NoIC-EP case) are also shown.

Despite the excellent agreement obtained in forward bias by both the full model (denoted as FM) and the case ignoring IC effects but using effective parameters (denoted as NoIC-EP), in Fig. 4 we show that only the former is able to correctly predict the behavior of the diode in reverse bias, especially for low voltages. To compare both approaches, we have performed calculations at 475 K, where we have already confirmed that the behavior of the diode is practically ideal and the FM is able to correctly reproduce the experimental results. In the figure, the measured values are compared with the total reverse current ($J_{reverse}$) obtained in both cases. The

thermionic (J_{th}) and tunnel (J_{tunnel}) contributions are also shown for completeness. In the absence of IC, the NoIC-EP case provides the expected bias-independent J_{th}, which is practically negligible as compared to J_{tunnel} in all the bias range. In the case of the FM, J_{th}, apart from being larger due to the barrier lowering, increases with the reverse bias as corresponds to the higher surface electric field. On the other hand, J_{th} is comparable or even higher than J_{tunnel} at the lower voltages. As concerns J_{tunnel}, it is substantially higher in the NoIC-EP case, mainly at the lower values of the reverse bias, due to the thinner energy barrier [see Fig. 5(b)]. The relative difference diminishes when the bias increases since a significant electron injection takes place at (lower) energies not so close to the top of the barrier. As a result of these differences, the total current is overestimated in the NoIC-EP case, mainly at the lowest voltages. We conclude that the FM, including the IC correction, is necessary to correctly reproduce the current in reverse bias.

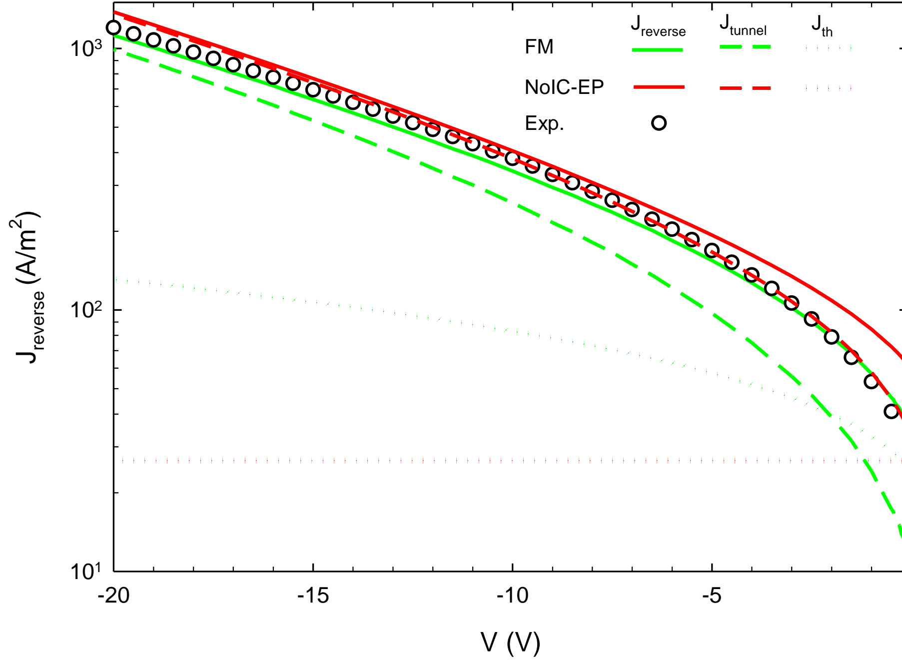

FIG. 4. Current density in reverse bias modeled including IC (FM, green lines) and without IC using effective parameters (NoIC-EP, red lines) as compared to measurements (circles). For the modeled values, the two ideal contributions, tunneling current (dashed lines) and thermionic emission (dotted lines), as well as the total reverse value (solid lines), are represented. T=475 K.

In order to understand the key role played by the barrier lowering associated to IC effects, and exploiting the capabilities of the model to provide a deep physical insight of injection processes in reverse bias, in Fig. 5 we compare, for a temperature of 475 K and a bias of -20 V, the details of electron injection as a function of energy and position in three case studies: (i) including IC effects (FM case), (ii) without including IC effects and using the same parameters as the FM (NoIC case), and (iii) without including IC effects but using the

effective parameters (NoIC-EP case). While cases (i) and (iii) provide similar values of the total reverse current (1.12×10^3 and 1.38×10^3 A/m^2, respectively, see Fig. 4), case (ii), by considering a too high barrier, obviously underestimates the current (0.34×10^3 A/m^2).

Fig. 5(b) shows the shape of the conduction band in each of the cases. At this temperature, $e\phi_B$=0.940 eV and $e\phi_B^{eff}$ =0.882 eV, and for a bias of -20 V, $e\Delta\phi_B$=0.123 eV. Thus, the maximum of the barrier ε_{Cmax} in the FM case is $e(\phi_B-\Delta\phi_B)$=0.817 eV. As expected, $e\phi_B^{eff}$ takes an intermediate value between $e\phi_B$ and $e(\phi_B-\Delta\phi_B)$. Fig. 5(a) shows the current injected per unit energy $J(\varepsilon)$, jointly with the transmission coefficient $T_C(\varepsilon)$ and the rate of incident electrons $N_m(\varepsilon)$. $T_C = 1$ once the energy is higher than ε_{Cmax}, corresponding to the range of thermionic emission, where, as expected, $J(\varepsilon)$ coincides in the three cases. For this bias, tunnel injection takes place mainly at energies fulfilling $\varepsilon - \varepsilon_{Fm} \gg k_B T$, so that $N_m(\varepsilon)$ exhibits the exponential behavior described by Eq. (6). It is remarkable that the average energy of the tunneled electrons is higher within the FM, fact that may have important implications for the precise calculation of the breakdown voltage (higher energies lead to earlier impact-ionization and avalanche). Finally, in Fig. 5(c) the transmission coefficient and the tunneling current per unit length are represented as function of the distance to the metal-semiconductor interface. The transmission coefficient of the two cases without IC is exactly the same since the barrier seen by carriers injected at a given position is identical in both cases. As observed, for this applied voltage, tunnel injection takes place mainly along the first 5-6 nm from the interface, slightly closer to the metal when IC is considered.

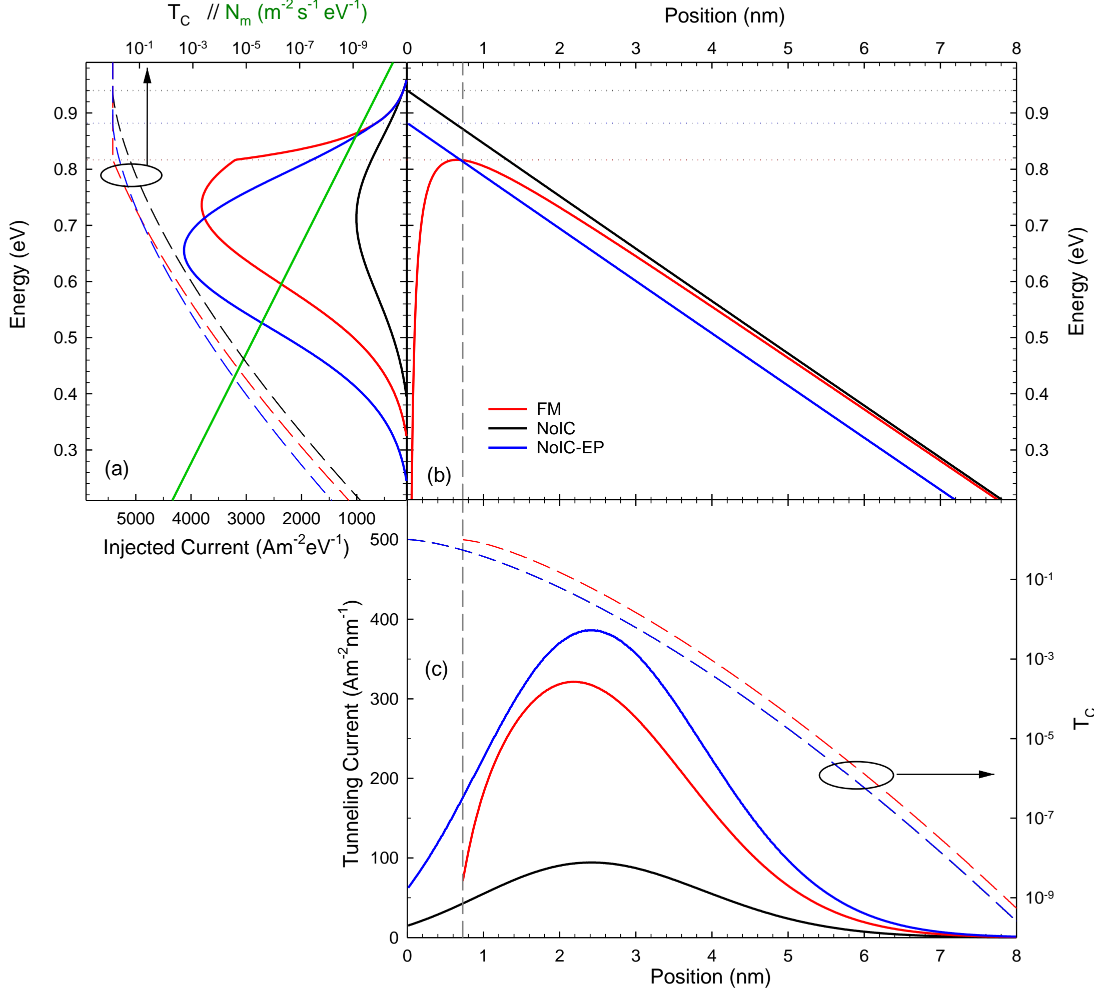

FIG. 5. Comparison of three case studies for T=475 K and V=−20 V: (i) including IC (FM, red lines), (ii) without IC and using the same parameters as the FM (NoIC, black lines) and (iii) without IC but using the effective parameters (NoIC-EP, blue lines). (a) Injected current (solid lines), transmission coefficient (dashed lines) and rate of electrons incident on the barrier (Eq. (6), green line) as a function of energy; (b) conduction band and (c) tunneling current (solid lines) and transmission coefficient (dashed lines) as a function of the distance from the metal-semiconductor interface. The horizontal dotted lines in (a) and (b) indicate the top of the barrier in each case, i.e., the energy separating tunneling and thermionic injection. The vertical dashed line in (b) and (c) indicates the position of the maximum of the barrier in the FM case.

Another test for the correctness of our model is the comparison with existing analytical models whose validity is restricted to some ranges of surface electric field values, like those of Murphy and Good[16] and Padovani and Stratton.[17] None of the mentioned models correspond exactly to our FM, since Padovani and Stratton ignore IC effects (thus, their model corresponds to our NoIC-EP case) and Murphy and Good ignore the effect of the doping (third term in the right-hand side of Eq. (1)). Our model, considering the appropriate terms, correctly reproduces the results of both models, as shown in Fig. 6 for the case of Murphy and Good's model at 300 and 475 K. We represent both the total and the tunneling current calculated by our model excluding the influence of the doping (which, on the other hand, could be significant for highly-doped SBDs

oriented to ultra-high-frequency applications). For the lower values of the electric field, Murphy and Good's thermionic emission current ($J_{TE}^{M\text{-}G}$), which, despite the name, includes also the tunneling contribution, is well reproduced by the total current obtained from our model. For intermediate electric fields, our model matches with the Murphy and Good's thermionic field emission current ($J_{TFE}^{M\text{-}G}$). Finally, for the higher electric fields, when electron injection takes place mainly near the metal Fermi level, our model fits accurately the analytical field emission current ($J_{FE}^{M\text{-}G}$). As observed, the lower the temperature, the lower the electric fields at which TFE and FE become dominant.

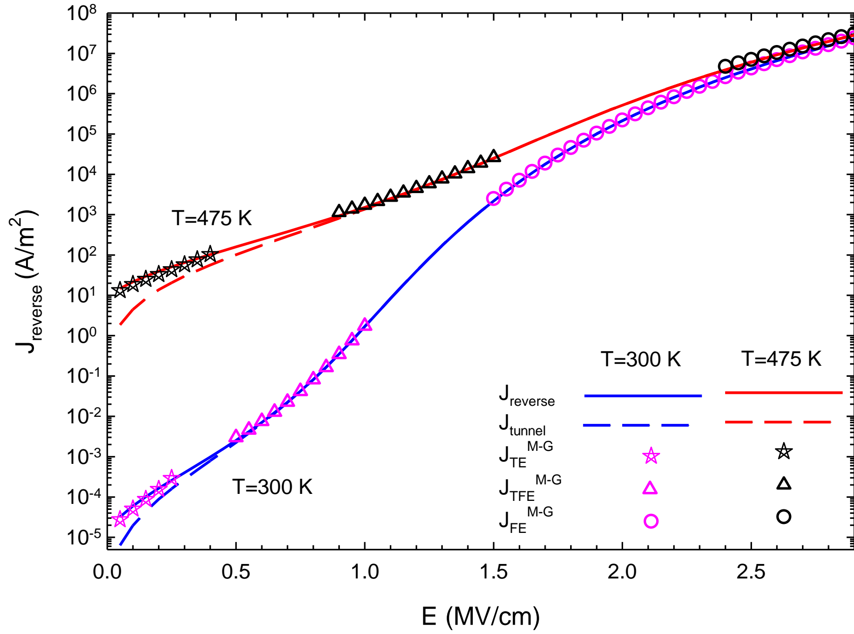

FIG. 6. Current density as a function of the surface electric field obtained by means of our numerical model (solid lines, total current; dashed lines, tuneling current) and by Murphy and Good's analytical model (symbols) for two temperatures, T=300 K (blue) and T=475 K (red). Murphy and Good's results are represented in the range of validity corresponding to the different current regimes: thermionic emission (TE, stars), thermionic field emission (TFE, triangles) and field emission (FE, circles).

To confirm that tunnel injection takes place at the expected energy regions when a good agreement between our model and that of Murphy and Good is achieved, Fig. 7 shows the injected current as a function of energy at T=300 K for surface electric fields of 0.20, 0.75 and 2.25 MV/cm, corresponding to the ranges of agreement with TE, TFE and FE currents, respectively. As observed, for 0.20 MV/cm, even if having some tunnel injection, the main current contribution is thermionic emission over the barrier, as expected in the TE regime; for 0.75 MV/cm, tunneling is already dominant and injection occurs not far from the top of the barrier, as corresponds to the TFE regime; and for 2.25 MV/cm it is localized around the Fermi level, as happens in the FE regime.

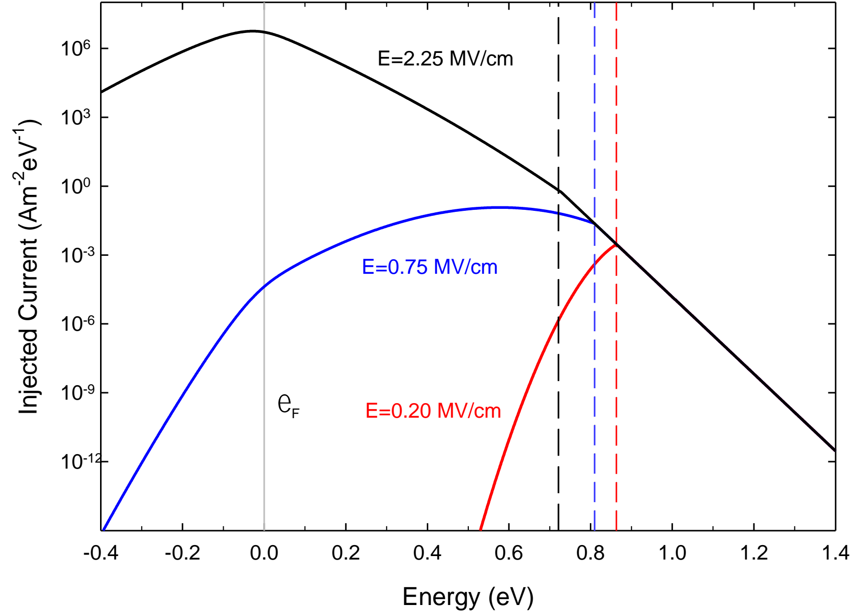

FIG. 7. Injected current as a function of energy for three different surface electric fields at 300 K. Vertical lines indicate the Fermi level and the energy corresponding to the top of the barrier in each case.

Once the model has been validated, it allows us to estimate the ideal leakage current due to thermionic emission and tunneling. Measured reverse current in excess of this ideal value indicate the presence of other leakage-current mechanisms, as happens in Fig.3(b) for temperatures below 425 K. Fig. 8(a) represents the experimental values of the current subtracting the two ideal contributions to the leakage current estimated by the model for different temperatures (in the range 300-475 K) and reverse-bias conditions (from -10 to -30 V). The excess current, while increasing with the reverse bias, does not change significantly with the temperature, thus allowing us to discard Poole-Frenkel emission and variable-range hopping mechanisms.[20] By representing this extra leakage current as a function of the inverse of the surface electric field for two different temperatures, 300 and 375 K (Fig. 8(b) and Fig.8(c), respectively), a quasi-linear dependence is identified. This dependence indicates that the mechanism leading to the extra leakage current could be tunneling assisted by traps.[20] From the slope of the dependence, energies of the trap level in the range 0.26-0.35 eV are identified (in particular 0.28 and 0.33 eV for 300 and 375 K, respectively).

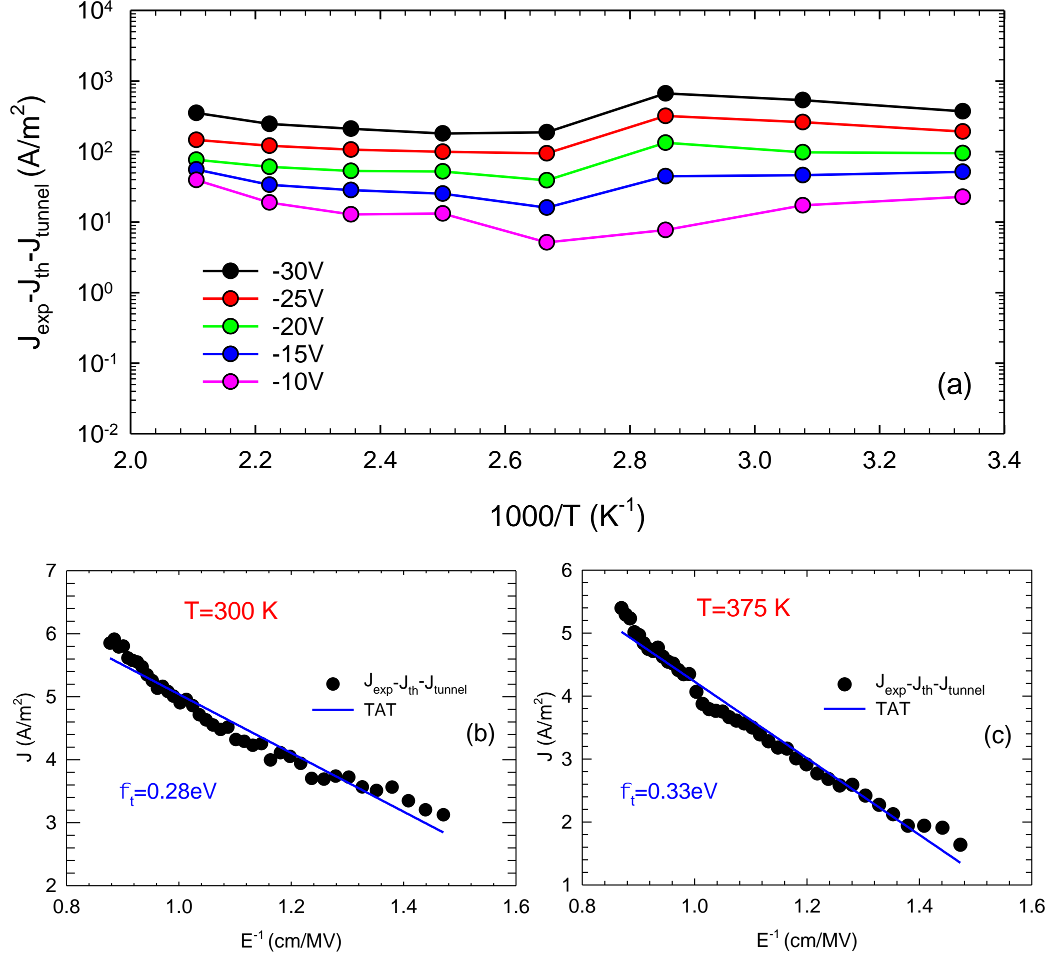

FIG. 8. (a) Reverse current density in excess of the ideal contributions as a function of 1/T (from T=300 K to T=475 K) for different values of reverse-bias voltage. Fitting of the results using the trap assisted tunneling (TAT) model for (b) T=300 K and (c) T=375 K.

V. CONCLUSIONS

A unified model for the calculation of ideal thermionic emission and tunneling currents in SBDs, including IC and doping effects, has been developed. The model addresses forward and reverse bias with the same set of physical parameters. Non-ideal effects related to the series resistance and the ideality factor are included in the thermionic emission current in order to achieve a good fitting of the forward-bias experimental curves. The values of the barrier height, series resistance and ideality factor are determined from such a fitting. The other parameters are the doping of the epilayer, calculated from the C-V curves, and the dielectric constant and the effective mass of the semiconductor, taken from the literature. Once the parameters are known, they are used to predict the diode behavior in reverse bias.

The model has been validated by comparison with current-voltage-temperature measurements performed in circular large-area GaN-on-SiC SBDs. An excellent fitting of the forward-bias *I-V* curves has been achieved in a wide range of temperatures (275-475 K). In reverse bias, at the highest temperatures, the current is quite close to the ideal value predicted by the model, but at temperatures lower than 425 K, a significant deviation from the ideal behavior has been found and identified to be possibly due to trap-assisted tunneling.

Apart from the determination of the characteristic parameters of the SBDs, the model allows assessing how ideal is the behavior of SBDs in reverse bias and which are the limits associated to a given technology. For example, it is possible to determine which is the voltage at which the ideal reverse leakage current reaches a given value limiting practical applications. It is also useful to evaluate the current in excess over the ideal value present in measurements in order to identify the leakage mechanisms at its origin, as done in the GaN diodes measured in this work.

ACKNOWLEDGEMENTS

This work has been partially supported through Grant PID2020-115842RB-I00 funded by MCIN/AEI/10.13039/501100011033. B. Orfao acknowledges the PhD contract from the Junta de Castilla y León. This work is also supported by the French ANR (Agence National de la Recherche) through the project SchoGaN (ANR-17-CE24-0034), the “Investissements d’Avenir” program GaNeX (ANR-11-LABX-0014) and the French network Renatech.

DATA AVAILABILITY

The data that support the findings of this study are available within the article.

REFERENCES

[1] T. W. Crowe, J. L. Hesler, E. Bryerton, and S. A. Retzloff, in Proc. IEEE Compound Semiconductor Integr. Circuit Symp. (CSICS), pp. 1-4 (2016).

[2] A. Semenov, O. Cojocari, H.-W. Hübers, F. Song, A. Klushin, and A.-S. Müller, IEEE Electron Device Lett. **31**, 674 (2010).

[3] F. Rettich, N. Vieweg, O. Cojocari, and A. Deninger, J. Infrared Millim. Terahertz Waves **36**, 607 (2015).

[4] A. S. Abdelrahman, Z. Erdem, Y. Attia and M. Z. Youssef, Can. J. Electr. Comput. Eng. **41**, 45 (2018).

[5] A. Ali, J. Chuanwen, Z. Yan, S. Habib and M. M. Khan, Energy Rep. **7**, 5059 (2021).

[6] H. Amano, Y. Baines, E. Beam, M. Borga, T. Bouchet, P. R. Chalker, M. Charles, K. J. Chen N. Chowdhury, R. Chu *et al.*, J. Phys. D. Appl. Phys. **51**, 163001 (2018).

[7] K. H. Teo, Y. Zhang, N. Chowdhury, S, Rakheja, R. Ma, Q. Xie, E. Yagyu, K. Yamanaka, K. Li and T. Palacios. J. Appl. Phys. **130**, 160902 (2021).

[8] K. Dang, J. Zhang, H. Zhou, S. Huang, T. Zhang, Z. Bian, Y. Zhang, X. Wang, S. Zhao, K. Wei, and Y. Hao, IEEE Trans. Power Electron. **35**, 2247 (2020).

[9] I. Mehdi, J. V. Siles C. Lee and E. Schlecth, Proc. IEEE **105**, 990 (2017).

[10] M.A. Ebrish, T. J. Anderson; A. D. Koehler; G. M. Foster; J. C. Gallagher; R. J. Kaplar, B. P. Gunning and K. D. Hobart, IEEE Trans. Semicond. Manuf. **33**, 546 (2020).

[11] S. M. Sze and K. K. Ng, *Physics of Semiconductor Devices* (John Wiley & Sons, New Jersey, 2007).

[12] K. Ejderha, S. Duman, C. Nuhoglu, F. Urhan and A. Turut, J. Appl. Phys. **116**, 234503 (2014).

[13] M. Gülnahar, Superlattices Microstruct. **76**, 394 (2014).

[14] W. Filali, N. Sengouga, S. Oussala, R. H. Mari, D. Jamee, N. Alhuda A. Saqri , M. Aziz, D. Taylor and M. Henini, Superlattices Microstruct. **111**, 1010 (2017).

[15] X. Guo, Y. Zhong, X. Chen, Y. Zhou, S. Su, S. Yan, J. Liu, X. Sun, Q. Sun and H. Yang, Appl. Phys. Lett. **118**, 243501 (2021).

[16] E. L. Murphy and R. H. Good, Jr., Phys. Rev. **102**, 1464 (1956).

[17] F. A. Padovani and R. Stratton, Solid State Electron. **9**, 695 (1966).

[18] J. Nicholls, S. Dimitrijev, P. Tanner and J. Han, Sci. Rep. **9**, 3754 (2019).

[19] W. Li, D. Jena, and H. G. Xing J. Appl. Phys. **131**, 015702 (2022).

[20] K. Fu, H. Fu, X. Huang, T. Yang, C. Cheng, P.R. Peri, H. Chen, J. Montes, C. Yang, J. Zhou, X. Deng, X. Qi, D. J. Smith, S. M. Goodnick and Y. Zhao, IEEE Journal Electron Devices Soc. 8, 74 (2020).

[21] X. Guo, Y. Zhong, X. Chen, Y. Zhou, S. Su, S. Yan, J. Liu, X. Sun, Q. Sun and H. Yang, Appl. Phys. Lett. **118**, 243501 (2021).

[22] J. Chen, Z. Liu, H. Wang, X. Song, Z. Bian, X. Duan, S. Zhao, J. Ning, J. Zhang and Y. Hao, Appl. Phys. Express **14**, 104002 (2021).

[23] G. Greco, P. Fiorenza, M. Spera, F. Gianazzo, and F. Roccaforte, J. Appl. Phys. **129**, 234501 (2021).

[24] J. Chen, Z. Liu, H. Wang, X. Song, Z. Bian, X. Duan, S. Zhao, J. Ning, J. Zhang, and Y. Hao, Appl. Phys. Express **14**, 104002 (2021).

[25] X. Kang, Y. Sun, Y. Zheng, K. Wei, H. Wu, Y Zhao, X. Liu, and G. Zhang, IEEE Trans. Electron Dev. **68**, 1369 (2021).

[26] K. Kim, D. Liu, J. Gong, and Z. Ma, IEEE Electron Device Lett. **40**, 1796 (2019).

[27] X. Guo, Y. Zhong, Y. Zhou, S. Su, X, Chen, S. Yan, J. Liu, X. Sun, Q. Sun, and H. Yang, IEEE Trans. Electron Dev. **68**, 5682 (2021).

[28] G. di Gioia, GaN Schottky Diodes for THz Generation, PhD Thesis, Université de Lille (2021).

[29] W. Li, D. Saraswat, Y. Long, K. Nomoto, D. Jena, and H. G. Xing, Appl. Phys. Lett. **116**, 192101 (2020).

[30] M. Hara, H. Tanaka, M. Keneko, and T. Kimoto, Appl. Phys. Lett. **120**, 172103 (2022).

[31] R. Fowler and E. A. Guggenheim, *Statistical Thermodynamics* (Cambridge University Press, New York, 1952), p. 460.

[32] N. F. Mott and. N. Sneddon, *Wave Mechanics and Its Applications* (University Press, Oxford, 1948), p. 23.